The Small Effect of Poroelastic Pressure Transients on Triggering of Production-Induced Earthquakes in the Groningen Natural Gas Field

Postma, Tom; Jansen, Jan Dirk

DOI
10.1002/2017JB014809

Publication date
2018

Document Version
Final published version

Published in
JGR Solid Earth

Citation (APA)
Postma, T., & Jansen, J. D. (2018). The Small Effect of Poroelastic Pressure Transients on Triggering of Production-Induced Earthquakes in the Groningen Natural Gas Field. *JGR Solid Earth*, *123*(1), 401–417. https://doi.org/10.1002/2017JB014809

AGU PUBLICATIONS

JGR

Journal of Geophysical Research: Solid Earth

RESEARCH ARTICLE

10.1002/2017JB014809

Key Points:

- Transient maxima in slip-promoting stresses were observed after abrupt changes in well rates in a poroelastic dynamic gas reservoir model
- Suddenly opening-up a well (or a cluster of wells) in the Groningen field can trigger an already (near)critically stressed fault
- The effect is so small that gradually opening-up a well may delay triggering seismicity but will most likely not prevent it from happening

Correspondence to:
J. D. Jansen,
j.d.jansen@tudelft.nl

Citation:
Postma, T., & Jansen, J. D. (2018). The small effect of poroelastic pressure transients on triggering of production-induced earthquakes in the Groningen natural gas field. *Journal of Geophysical Research: Solid Earth*, *123*. https://doi.org/10.1002/2017JB014809

Received 1 AUG 2017
Accepted 4 DEC 2017
Accepted article online 13 DEC 2017

The Small Effect of Poroelastic Pressure Transients on Triggering of Production-Induced Earthquakes in the Groningen Natural Gas Field

Tom Postma[1] and Jan-Dirk Jansen[1]

[1] Department of Geoscience and Engineering, Delft University of Technology, Delft, Netherlands

Abstract Over the past decade, a steep increase in the number of seismic events has been observed in the Groningen gas field, the Netherlands. It is generally accepted that these are induced by compaction of the reservoir rock due to extensive depletion, causing a buildup of strain energy in faults that may be released seismically. We address the possible triggering of fault slip by the transient pressure field surrounding a well that has undergone a sudden rate change. Assuming a unilateral decoupling between displacement and pressure, numerical experiments are conducted using a sequential finite volume-finite element solution strategy that fully incorporates second-order terms in the radial flow equation. We investigate an idealized Groningen-like geometry to discover whether the hypothesized possibility of triggering-induced seismicity exists, explore how some controllable and uncontrollable variables influence its severity, and possibly provide clues on how production strategy might be able to avoid its occurrence. The results demonstrate that sudden production changes can indeed trigger near-well seismic events, but that the effect is very small compared to other potential causes. Changing from sudden to gradual changes in well rates is therefore not expected to lead to a significant reduction in the number or magnitude of production-induced earthquakes in the Groningen field.

Plain Language Summary Natural gas production from the Groningen field in the Netherlands increasingly causes small earthquakes that lead to significant damage to houses, feelings of insecurity, and social unrest. It has been suggested that sudden changes in production (opening or closing wells) may trigger such earthquakes. The results in this paper demonstrate that sudden production changes do indeed have an effect on the stresses in faults, that is, that they can trigger earthquakes, but that the effect is very small compared to other potential causes. Changing from sudden to gradual changes in well rates is therefore not expected to lead to a significant reduction in the number or magnitude of production-induced earthquakes in the Groningen field.

1. Introduction

We consider earthquakes induced or triggered by natural gas production from subsurface reservoirs. These belong to the broad category of seismic events caused by anthropogenic injection or extraction of fluids in subsurface rock formations (Dahm et al., 2015; Ellsworth, 2013; Grasso, 1992; Grigoli et al., 2017; McGarr et al., 2002; Segall, 1989; Shapiro, 2015; Zbinden et al., 2017). In this broad category, various mechanisms are at play. A first distinction concerns the source of energy released by the fault movement. This may be elastic rock deformation originating from plate tectonics ("triggered" earthquakes) or production-induced compaction or injection-induced expansion of reservoir rock ("induced" earthquakes). A second distinction concerns the location of the seismic event in relation to the reservoir into which or from which fluids are injected or extracted. Fault movement may be triggered in the reservoir itself or in the overlying or underlying impermeable cap or base rock. A third distinction concerns the pathway for the propagation of pore pressure from the injection or production well to the fault. This may be a (predominantly) natural fracture network, as is the case for geothermal heat production from hot fractured rock, or a fracture network generated by hydraulically stimulating or "fracking" relatively impermeable rock as applied in shale gas production. Alternatively, the pathway for pore pressure propagation may be (predominantly) the reservoir matrix, that is, the permeable rock, as is often the case for "conventional" oil and gas production.

We restrict our analysis to the subset of induced earthquakes that originate from the reservoir itself, with a main pathway for pore pressure propagation formed by permeable rock with little to no fractures such that the flow is governed by Darcy's law. In particular, we consider earthquakes related to natural gas production that have been observed in the large Groningen gas field in the Netherlands (Bourne et al., 2014; Dempsey & Suckale, 2017; De Waal et al., 2015; Grasso, 1992; Lele et al., 2016; Mulders, 2003; Nepveu et al., 2016; Pijpers, 2017; Sanz et al., 2015; Van Thienen-Visser & Breunese, 2015; Van Wees et al., 2014; Wassing et al., 2016). The field has estimated recoverable reserves of 2.8×10^{12} Sm^3, of which 2.0×10^{12} Sm^3 have been produced to date through a total of 258 wells distributed over 22 clusters. At the start of production reservoir pressure was 35 MPa, which has dropped to a current average pressure of around 7.5 MPa, although at present a differential pressure of approximately 2.5 MPa exists between the north and south of the field (approximately 45 km apart) because of a spatially phased development and regional production restrictions. Seismic activity with magnitudes above 2.5 M_L was not observed until the early 1990s, but over the past decade a steep increase in the number of events has occurred, with a maximum observed event of 3.6 M_L in 2012. It is now generally accepted that most of the energy in the seismic events in the Groningen field results from compaction of the sandstone reservoir rock, although the release of additional seismic energy from naturally stressed faults deep below the reservoir cannot be completely excluded. The most likely hypothesis is that differential compaction, and compaction at both sides of normal faults with significant throws are the main reasons for the buildup of strain energy that may be released when the shear stresses in the faults reach a critical limit caused by continuing compaction (Lele et al., 2016; Mulders, 2003; Van Wees et al., 2014; Zbinden et al., 2017). An alternative explanation for the triggering of normal faults is poroelastic compaction in case of specific reservoir properties (high Biot coefficient and low Poisson ratio), as described by Zoback, (2007, chapter 12 and references therein). However, a recent inverse parameter study by Dempsey and Suckale (2017) indicates that such poroelastic compaction would require unrealistic parameter values and that, likely, other mechanisms are (also) at play.

The current seismic hazard model as applied by the operator is based on a statistical relationship between the cumulative compaction and the event rate (Bourne et al., 2014). Control measures, imposed at national government level and based on advice of the national regulatory authority (the State Supervision of the Mines) primarily involve reducing production rates field wide, and in particular at clusters where high event rates have been observed (De Waal et al., 2015). Statistical analysis indicates that these production rate restrictions indeed show a correlation to a reduced event rate, although convincing evidence specifically indicating a direct causal relationship has yet to be put forward (Nepveu et al., 2016; Pijpers, 2017; Van Thienen-Visser & Breunese, 2015). Furthermore, it has been hypothesized that another control measure could be the avoidance of fluctuations in well production rates, both in the form of sudden changes (production start-ups or close-ins) and in the form of seasonal fluctuations. In fact, the current government-imposed production controls are already based on this hypothesis: they limit the fluctuation of production rates to a minimum, but such that seasonal variations in domestic natural gas demand (notably increased production in cold winters) can be accommodated. This implies a flat production rate in combination with storage of excess gas in summer in a nearby depleted gas field that is now used as an underground gas storage facility.

The existing studies into production-induced seismicity in the Groningen field can all be characterized as "quasi-static," that is, they implicitly assume that the dynamic response of the reservoir to pressure decline before the occurrence of a seismic event is much slower than the typical dynamics of a reservoir responding to sudden changes in production. A recent generic study into gas production-induced seismicity by Zbinden et al. (2017) demonstrates the significance of multiphase flow and, in particular, the late effects of fluid flow into fault zones (on a timescale extending to the order of decades). A study into similar effects resulting from produced-water injection has been reported by Segall and Lu (2015). In the present study, we address the direct changes (on a timescale of days) in the normal and shear stresses in faults originating from sudden rate changes in neighboring wells. The changes are governed, at least to first order, by the "slow" poroelastic pressure transient behavior of the reservoir, that is, by the dynamics of fluid pressures in the reservoir rock and the faults taking into account the elasticity of the fluid and the rock (Biot, 1941). After occurrence of an event, the dynamic response of the reservoir is governed by the "fast" poroelastic behavior of the reservoir (on a timescale in the order of seconds), in which the dynamics of the moving rock, in combination with the pressure dynamics, play a leading role (Biot, 1956). Stress waves traveling through the reservoir may trigger new events at other locations, a phenomenon well known from tectonic earthquakes. Such events may occur in the same fault where the initial event took place, leading to a gradually extending region of partial stress release in that fault, or in faults at a larger distance.

In our study we do not address these fast poroelastic effects. Neither do we consider the gradual pressure decline that forms the root cause of production-induced seismicity nor long-term pore pressure diffusion effects. Instead, we consider the near-immediate (on a timescale of days) stress changes in a fault that is critically, or almost critically, stressed such that a small perturbation of the local stress state may lead to triggering of an earthquake. In particular, we are interested in slow poroelastic pressure transients in the Groningen field resulting from a sudden increase in production rate in a well. We note that our study is restricted to single-phase gas flow and elastic reservoir behavior. It has been shown by Zbinden et al. (2017) that multiphase (gas-water) effects are important at larger timescales, while the same holds for the plastic behavior of cap rock (flowing salt) as investigated by Zbinden et al. (2017) and Orlic and Wassing (2013). Our approach therefore provides a first-order assessment of the relevance of pressure-transient-related stress changes on the triggering potential of production-induced seismicity.

Among others, Wang (2000), Shapiro (2015), and Cheng (2016) present analytical 3-D solutions of the propagation of pore pressures and stresses resulting from sudden rate changes in a point source for a poroelastic full space, following the work of Rudnicki (1986) who, in turn, builds on results of Cleary (1977). For a permeable reservoir of large spatial extent sandwiched between impermeable cap rock and base rock layers, an axially symmetric schematization appears more appropriate. Such (semi)analytical solutions in cylindrical coordinates for the propagation of pore pressures around a line source or sink have been derived in various domains such as hydrology (Bear & Corapcioglu, 1981; Helm, 1994; Jacob, 1940; Sternberg, 1969; Theis, 1935; Verruijt, 2016), petroleum engineering (Clegg, 1967; Monfared & Rothenburg, 2015b; Van Everdingen & Hurst, 1949), geotechnical engineering (Carter & Booker, 1982), geomaterials (Rudnicki, 1986), and geophysics (Segall & Fitzgerald, 1998). Several of these publications also consider the resulting stresses and/or strains in axial and/or radial directions using different solution methods (both direct and Laplace-transformed, the latter with either fully analytical or numerical inverse transforms). Importantly, they use a variety of assumptions regarding the domain extent (bounded versus infinite), boundary conditions (constant rate versus constant pressure) and deformation state (1-D with axial or radial deformations only versus 2-D under plane stress or plane strain conditions). There are some publications in which it is attempted to justify the various assumptions with the aid of numerical simulations (Hsieh & Cooley, 1995; Monfared & Rothenburg, 2015a).

For this study, the slow poroelastic response to a transient flow regime is modeled numerically in a radially symmetric domain. We use a cell-centered finite volume method (FVM) to simulate the flow, and a vertex-centered finite element method (FEM) to simulate linear poroelastic deformation. The high flow rates that we consider and the high compressibility of natural gas, especially at low pressures as may occur when the reservoir approaches depletion, require special care of the fluid formulation to incorporate pressure-dependent expansion effects. To this end, we make use of a so-called "real-gas pseudopressure" formulation as originally introduced by Al-Hussainy et al. (1966) for use in analytical solutions for the flow of real gases in porous media. We investigate an idealized Groningen-like geometry, solving for short timescales to capture the developing pressure field of a single producer and the stress changes it induces. The aim is to discover whether the hypothesized possibility of triggering-induced seismicity exists, explore how some controllable and uncontrollable variables influence its severity, and possibly provide clues on how production strategy might be able to avoid its occurrence.

2. Poroelastic Modeling

We consider an axially symmetric, laterally extensive, horizontally layered geometry modeled on the local geology of the Groningen gas field. Due to the compressibility contrast between pore fluid and reservoir rock, coupling of the flow problem to the geomechanical problem can be neglected. This enables the use of an efficient sequential FVM-FEM solution strategy in our dynamic reservoir simulator, in which the cell-centered pressure field acts as a known body force when solving for the vertex-centered solid displacements. These displacements can subsequently be used to determine the complete state of stress as a function of time and spatial coordinates.

2.1. Governing Equations

2.1.1. Fluid Flow

The basic governing equation of poroelasticity is the storage equation,

$$\alpha \frac{\partial \varepsilon}{\partial t} + S\frac{\partial p}{\partial t} - \nabla \left(\frac{k}{\mu} \nabla p \right) = 0 \tag{1}$$

where ε is the volume strain, α is the Biot coefficient, S is the storativity, and the third term represents the total fluid flux with respect to the porous medium via Darcy's law. For a full derivation starting from conservation laws, see, for example, Wang (2000) and Verruijt (2016). Equation (1) signifies mass conservation of both pore fluid and the solid matrix and is obtained by adding both mass balance equations after normalizing them by the density of the conserved quantity they represent. In this expression, second-order terms have been dropped, which is justified if the product of velocity and density gradient of each conserved quantity is negligibly small. The equation has a form resembling a classical diffusion equation in terms of pressure p, augmented with terms that account for the effect that deformation of the porous medium has on the flow problem.

If a large contrast exists between the fluid (gas) compressibility C_g and the compressibility of the (drained) porous medium C_m such that $C_m = \frac{1}{K} \ll \phi C_g$, the influence of solid deformation on the pressure solution can be safely neglected (Cheng, 2016). (Here K is bulk modulus and ϕ is porosity.) The reverse does not hold, that is, pore pressure changes must be taken into account when solving for solid displacements. This unilateral decoupling of flow from mechanics allows for the flow problem to be solved separately, after which the obtained pressure field enters the deformation problem as a known body force.

However, the assumption that second-order terms can be neglected—although valid for slightly compressible fluids and low flow velocities—is generally untenable when describing the radial flow of gas, especially for the high flow rates that occur around a producing gas well. Fortunately, the decoupling allows us to rewrite the pore fluid mass balance as a diffusion equation without dropping these terms, by introducing a "real-gas pseudopressure" as proposed by Al-Hussainy et al. (1966):

$$m(p) = 2 \int_{p_{\mathrm{ref}}}^{p} \frac{k}{\mu_g(p)} \frac{p}{Z(p)} \,\mathrm{d}p\,, \tag{2}$$

where k is permeability, μ_g is gas viscosity, Z is the real gas deviation factor, and p_{ref} is a sufficiently low reference pressure, chosen such that it is always beneath the lowest pressure in the system. Equation (2) represents a "Kirchhoff transformation" that (partly) linearizes the governing equations for compressible porous-media flow in analogy to similar transformations introduced much earlier to linearize equations for flow of heat through solids (Kirchhof, 1894). Using the real gas equation of state, the fluid mass balance equation can be rewritten in terms of p and Z. Assuming Darcy flow, constant porosity, and isothermal conditions, a change of variables to $m(p)$ gives the following (nonlinear) diffusion equation:

$$\frac{\phi \mu_g(p) C_g(p)}{k} \frac{\partial m}{\partial t} - \nabla^2 m = 0\,, \tag{3}$$

which describes the flow of gas without assuming small density gradients and low flow rates, while fully incorporating the pressure-dependent fluid properties. The pseudopressure $m(p)$ is precomputed to a desired degree of accuracy using numerical integration, so that upon obtaining a solution for m, the real pressure solution p can be obtained by linear interpolation without introducing significant extra errors.

2.1.2. Solid Mechanics

The displacement problem must satisfy the equations of mechanical equilibrium, which follow from Newton's laws of motion when the second derivative of the displacement vector $\mathbf{u}$ with respect to time (i.e., the change in momentum) is assumed to be negligible:

$$\boldsymbol{\nabla} \cdot \boldsymbol{\sigma} - \boldsymbol{f} = \mathbf{0}, \tag{4}$$

where $\boldsymbol{\sigma}$ is the second order Cauchy stress tensor and $\boldsymbol{f}$ represents the body forces in all coordinate directions, if present. Following the convention used in soil mechanics, normal stresses are positive for compression, and a shear stress σ_{ij} is positive when it applies force in a direction along j of opposite sign compared to the

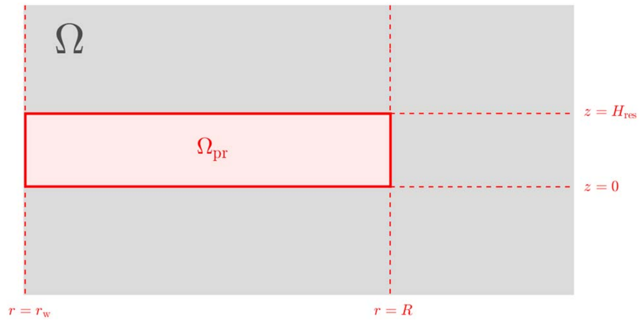

Figure 1. Subdomain Ω_{pr} embedded within the complete system Ω, which extends further in the positive radial and both vertical directions.

component n_j of the unit vector normal to the surface on which it acts. Besides the equations of equilibrium, the problem must satisfy the strain-displacement relations (or compatibility equations),

$$\boldsymbol{\varepsilon} = \frac{1}{2}\left[\nabla \mathbf{u} + (\nabla \mathbf{u})^T\right], \tag{5}$$

where $\boldsymbol{\varepsilon}$ is the infinitesimal strain tensor. Lastly, stress and strain are linearly related via Hooke's law in the constitutive relations

$$\boldsymbol{\sigma} = \mathbf{C} : \boldsymbol{\varepsilon}, \tag{6}$$

where $\mathbf{C}$ is a rank 4 stiffness tensor. For a three-dimensional isotropic material, this amounts to 21 equations in total (6 equilibrium equations, 9 strain-displacement relations, and 6 independent constitutive equations), one for each of the unknowns (3 displacements, 9 stresses, and 9 strains).

2.2. Numerical Solution

Simulations were conducted in Matlab using an algorithm adapted from Chessa (2002) for an unstructured triangular grid, which is initialized using Matlab's built-in Delauney-type meshing algorithm and finished by alternating steps of refinement and node coordinate adjustment to improve triangle shape. The pseudopressure problem is solved on only part of the domain, chosen as a section of the reservoir interval of an extent such that flow remains infinite acting during simulation. An especially high grid cell resolution is chosen in this region to fully capture the developing pressure field.

2.2.1. Pressure Field

Given that the reservoir is in a transient flow regime, at each time t after the start of production there exists a radius r beyond which the disturbance has not yet had time to travel, that is, pressure is still constant at $p = p_{\mathrm{res},0}$. For sake of computational efficiency, we choose a radius $r = R$ bounding the subdomain Ω_{pr} outside of which the diffusivity equation (3) needs not be solved; see Figure 1. Within Ω_{pr}, a high grid cell resolution enables us to capture the steep gradients of the developing pressure field. The problem is discretized in time using backward differences to ensure numerical stability. Discretization in space is achieved with the finite volume method, Ω_{pr} being divided into $n_{\mathrm{e,pr}}$ grid cells each containing a discrete pseudopressure unknown m_k. Pseudoflow across cell faces is described using a two-point flux approximation as described by Karimi-Fard et al. (2003). Grouping of terms results in a nonlinear system of $n_{\mathrm{e,pr}}$ equations for which Picard iteration was found to be of sufficient computational efficiency.

2.2.2. Solid Displacements and State of Stress

The mechanical problem is then solved across the entire domain Ω using the Galerkin method of weighted residuals, with discrete unknowns $u_{r,i}$ and $u_{z,i}$ at each of the n_{n} nodes, located at triangle vertices. Making use of the linearity of the problem, the effect of pressure changes in the reservoir is incorporated by assigning every element l a pressure drop Δp_l, with $\Delta p_l = p_{k_l} - p_{\mathrm{res},0}$ for each element on Ω_{pr} and zero otherwise.

Upon solving for the displacement field, the state of stress can be computed using the compatibility equations (5) and Hooke's law (6). As the displacement gradients (and consequently the stress components) are generally not continuous across cell boundaries, the average state of stress in an element is chosen as a representative value. Using direction cosines, the reference frame can be rotated to find the stress components acting on a hypothetical plane at a given angle.

To assess the potential for triggering of production-induced seismicity, we use the Coulomb stress $\tau_{\mathrm{c}} = \tau_{\mathrm{s}} - \mu_{\mathrm{f}} \cdot \sigma'_{\mathrm{n}}$, with μ_{f} the coefficient of friction, σ'_{n} the effective normal stress acting on the fault, and τ_{c} the magnitude of the shear stress promoting fault slip. Given the employed sign convention and the fact that Groningen is in a normal faulting regime, this implies a sign change when assessing faults dipping toward the producer.

2.3. Reservoir Model

2.3.1. Geometry and Rock Properties

Numerical experiments were performed for an axially symmetric, horizontally layered geometry, with the producing interval sandwiched between impermeable overburden and basement. Stratigraphy was based on the geology of the gas-producing regions of the northern Netherlands; see Figure 2.

Elastic and hydromechanical properties were obtained from the technical addendum to the field development plan published by the operator responsible for extraction of oil and gas in the the Groningen field (Nederlandse Aardolie Maatschappij, 2016). Elastic properties are constant within stratigraphic intervals,

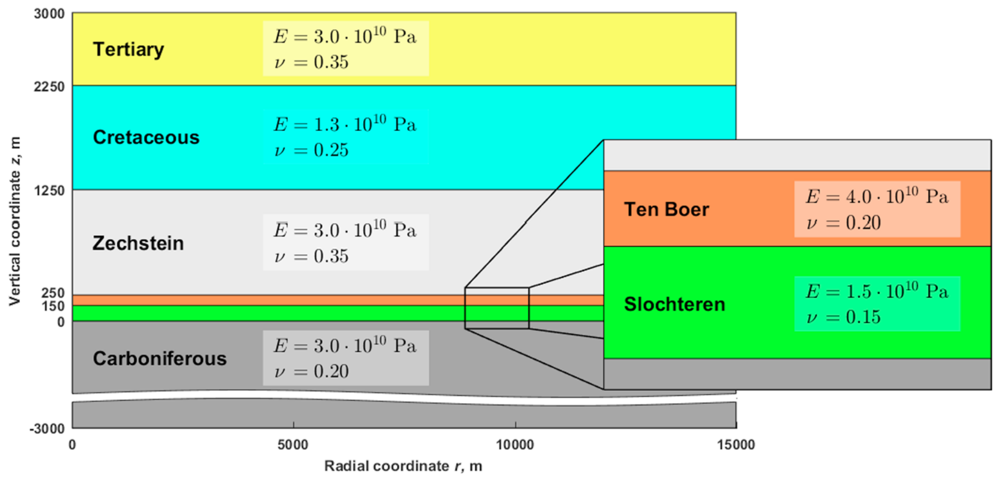

Figure 2. Horizontally layered stratigraphic model with corresponding elastic parameters.

and the producing interval was modeled with a homogeneous permeability ($k = 5 \cdot 10^{-14}\mathrm{m}^2$) and porosity ($\phi = 0.15$). To compute the Coulomb stresses, we used a friction coefficient $\mu_f = 0.6$.

Zero-displacement boundary conditions were applied at the proximal and bottom domain boundaries in radial and vertical directions, respectively. All other boundary conditions were left stress free. Lateral extent of the whole geometry and vertical extent of the modeled underburden were chosen such that a further increase in size no longer influenced the outcome of numerical experiments.

2.3.2. Fluid Properties

The pore fluid was modeled as a gas mixture typical for the Groningen field, with specific gravity $\gamma_g = 0.65$ and a methane content of around 80%. Pressure-dependent properties of reservoir fluids are usually best described by empirical correlations relating them to pseudo reduced temperature T_{pr} and pseudo reduced pressure p_{pr}, computed by normalizing pressure and temperature with their respective (pseudo)critical values T_{pc} and p_{pc} (in our study 187 K and 4.46 MPa respectively). Pressure-dependent gas viscosity μ_g was modeled using Lucas' approximation (Lucas, 1981) to the correlation charts put forward by Carr et al. (1954), valid for $1 < T_{pr} < 40$ and $0 < p_{pr} < 100$. The explicit correlation proposed by Azizi et al. (2010) (valid for $1.1 < T_{pr} < 2$and $0.2 < p_{pr} < 11$) was used to compute the real gas deviation factor Z as a function of pressure. Besides its accuracy, its explicit nature allows it to be differentiated to derive an analytical expression for the pressure-dependent isothermal compressibility C_g.

3. Results

3.1. Transient Baseline Scenario

As a base case, we consider the scenario of a disk-shaped gas reservoir at a constant initial pressure $p_{res,0} = 7.5$ MPa, comparable to current pressures found in Groningen. At the start of production, a rate constraint of $q_{sc} = -3.0 \cdot 10^6$ m^3/day is applied instantaneously to the proximal boundary of the producing interval. Using a time step Δt of 15 min, simulations model the first 5 days of production.

3.1.1. Pressure Field

Figure 3 visualizes the development of the pressure field during the first 5 days of production, showing that flow is still infinite acting. The subdomain Ω_{pr} is modeled with a radius $R = 2,500$ m, in which this transient regime can be modeled for up to 20 days.

3.1.2. Displacements

As pore pressure in the reservoir diminishes, effective stresses change and the reservoir deforms. For larger timescales with field-wide pressure drops, displacement in the negative z direction tends to dominate: the overburden can subside as one unit with minimal strain while the basement has no free surface enabling this behavior. At short times, however, we can still

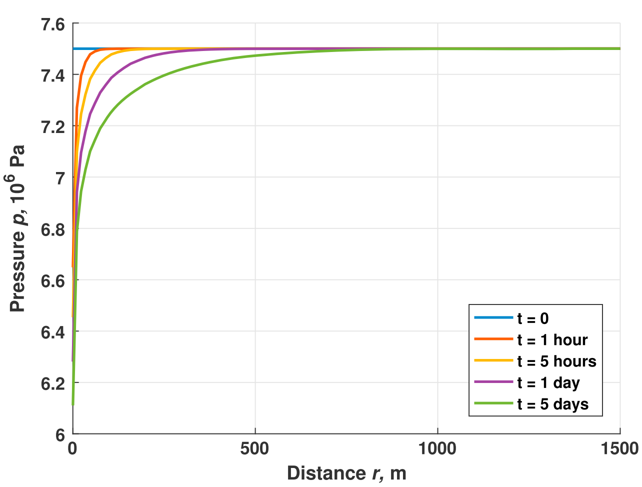

Figure 3. Developing pressure field during the first 5 days of production.

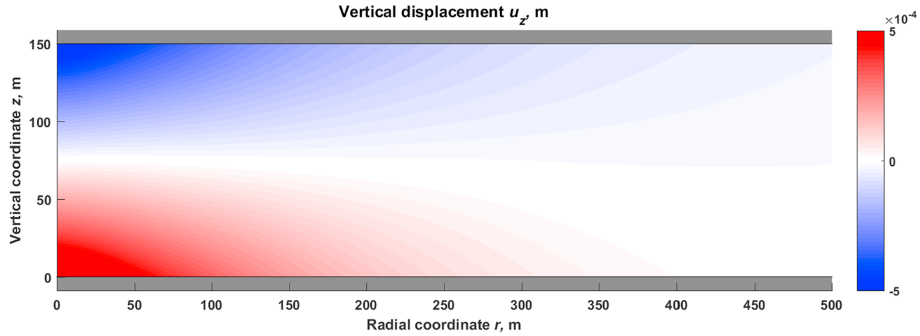

Figure 4. Vertical displacement field after 1 day of production.

observe that positive vertical displacement at the bottom of the reservoir is of the same order of magnitude; see Figure 4. The reason for this is that, as the pressure disturbance has only traveled a small distance into the reservoir, the arching effect works to prevent vertical displacement (Mulders, 2003).

Unlike the vertical displacement, the radial displacement is not monotonous along the radial axis for an infinite-acting flow regime: a state of relative compression (i.e., decreasing radial displacements) is found near the wellbore, changing to relative extension (i.e., increasing radial displacements) with increasing radial coordinate; see Figure 5.

3.1.3. Stress Field

Plotting the Coulomb stress on a fault dipping toward the producer at $\theta = 85°$ as a function of both spatial coordinates, Coulomb stress is found to concentrate at the top of the reservoir; see Figure 6. Conversely, Coulomb stresses on faults dipping away from the producer show elevated levels local to the bottom of the reservoir. This is due to the different sign of shear stress on both vertical boundaries, as well as to an asymmetry in the relative magnitude of shear and normal stresses caused by rotating the reference frame. Due to the nature of the trigonometric functions required for the transformation, the asymmetry decreases for decreasing dip angles, vanishing for $\theta = 60°$ after which a further decrease of θ causes the same asymmetry to develop on the other side.

Knowing that the state of stress is most conducive to fault slip at either the top or bottom of the reservoir interval, the Coulomb stress can be visualized as function of time and radial coordinate by only looking at the high-risk zone; see Figures 7 and 8. After approximately a day of production, the Coulomb stress exhibits a local maximum around $r = 100$ m. This location then remains the spatial maximum as production continues and the pressure field stabilizes.

To facilitate comparison of Coulomb stress responses when changing the value of a certain parameter, a two-dimensional data set was created by plotting τ_c only for radial coordinate r where the maximum occurs. Figure 9 shows the result for the stress field described above, as well as the components of normal and shear stress from which it is derived. It becomes clear that the (sudden) increase in Coulomb stress arises because, although the shear contribution immediately grows in magnitude, the initial change in effective normal stress (due to elastic coupling) is one of relative tension. Starting from the moment at which the pressure disturbance

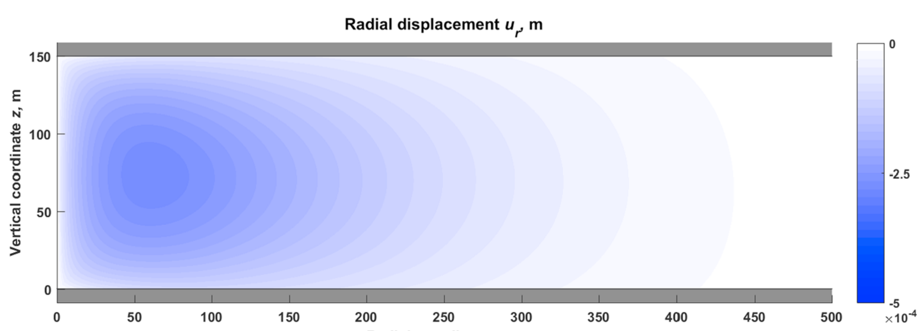

Figure 5. Radial displacement field after 1 day of production.

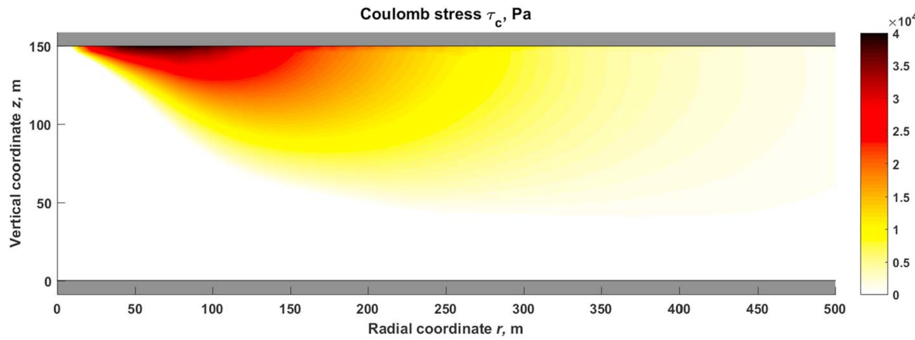

Figure 6. Coulomb stress for slip along a fault plane dipping toward the producer at $\theta = 85°$ at an arbitrary location, $t = 1$ day.

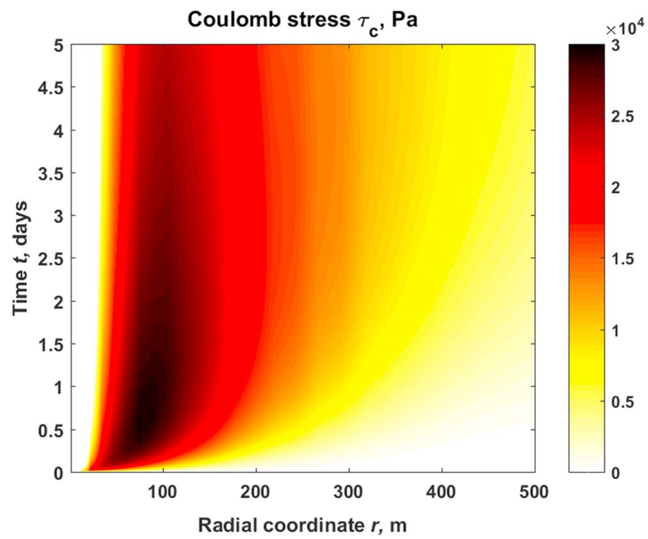

Figure 7. Coulomb stress versus time t and radial coordinate r at the top of the reservoir, for a plane dipping toward the producer at $\theta = 85°$, first 5 days.

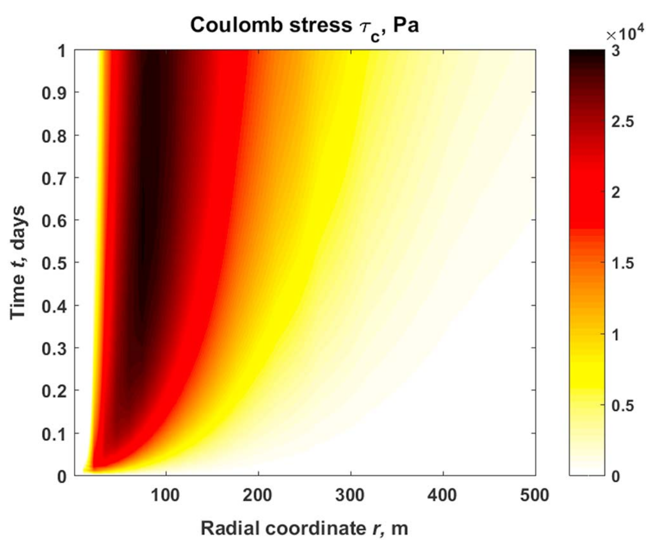

Figure 8. Coulomb stress versus time t and radial coordinate r at the top of the reservoir, for a plane dipping toward the producer at $\theta = 85°$, first day.

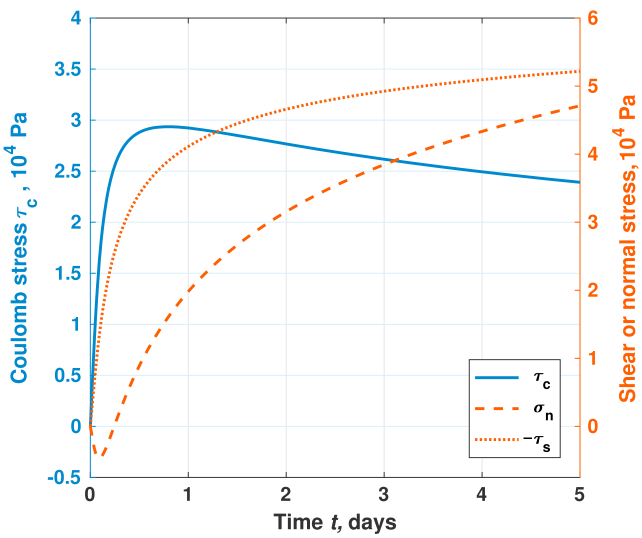

Figure 9. Coulomb stress and its components during the first 5 days of production, note the initially tensile σ_n.

arrives, the drop in pore pressure makes a compressive contribution to effective normal stress σ_n. Eventually, compressive stresses come to dominate the tensile stress transferred via the rock matrix, stabilizing the Coulomb stress; see Figure 10.

3.1.4. Dependence of Coulomb Stress on Fault Orientation

To explore the influence of fault orientation on both the magnitude and prominence of the local maximum in Coulomb stress, simulations were conducted for various dip angles and directions (i.e., dipping toward the center or the edge of the reservoir), again assuming normal faulting. Faults in the Groningen field are often especially steep, with dip angles generally around 80° and seldomly below 70° (Nederlandse Aardolie Maatschappij, 2016). Figure 11 shows the variation of Coulomb stress response, which exhibits an upward trend in both magnitude and prominence of the local stress maximum for increasing dip angles, as well as an increasing asymmetry between the different dip directions. As very large dip angles (i.e., near-vertical faults) are not uncommon and this orientation shows the strongest response, a fault dipping toward the producer at $\theta = 85°$ is selected as the subject of further numerical experiments. We did not explicitly investigate the effect of strike of the fault, that is, all results are valid for points on the fault that are oriented perpendicular to the radial coordinate. An analysis not reported here revealed that the strongest changes in Coulomb stresses occur just there.

3.2. Production Rate

Lowering production rates is often viewed as a seemingly obvious way of mitigating earthquake risk. Figure 12 shows the Coulomb stress response for different production rates, indeed showing greater stress levels for higher well rates. In fact, both peak stress and the stabilizing tails of the curve appear roughly proportional to the applied well rate. Separating the Coulomb stress into its normal and shear components (see Figure 13), it becomes clear that the increased Coulomb stress can be ascribed mostly to a greater shear stressing rate caused by the steeper pressure gradients required to satisfy the production constraint. Although normal stress drops to a lower minimum for higher production rates, the timing of this minimum and the moment when the pore pressure drop succeeds in bringing back a state of relative compression remain the same.

3.3. Production Ramping

An instantaneous switch in well rate to operating levels is hypothesized to increase the risk of triggering earthquakes compared to a more gradual approach, that is, either moving to operating rates in two or more discrete steps or in a continuous rate buildup, both of which can be applied in a shorter or longer time window. Both parameters were varied separately to study their effect on stress levels, choosing the moment at which production commences such that the total amount of gas produced is equal when the ramping phase is complete. In both cases, the stress levels appeared to remain below or equal to the stresses found for an instantaneous switch to operating rate, the curves meeting up as their respective pressure fields begin to align. For the case of a varying number of pressure increments within the same time window (see Figure 14), the maximum Coulomb stress was observed to be slightly lowered as the number of increments increases. However, this change seems to be governed only by the amount of extra time taken to reach the operating rate. Indeed, increasing the time Δt between the onset of production and the moment that operating rates are reached moves the maximum Coulomb stress along the descending curve, with a time offset that seems proportional to Δt; see Figure 15.

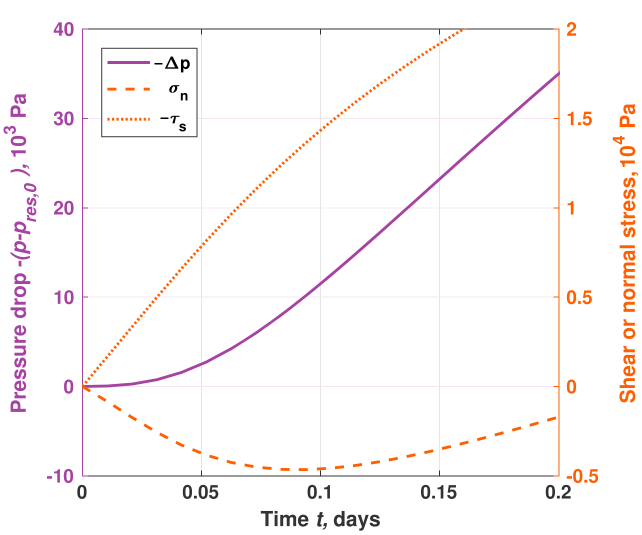

Figure 10. Stress components superimposed on pressure drop during the first 0.2 day of production.

3.4. Reservoir Pressure

The frequency with which production-induced seismic events occur in the Groningen gas field has seen a very sharp increase over the past decades, a trend that might be explainable in part by ever-increasing levels

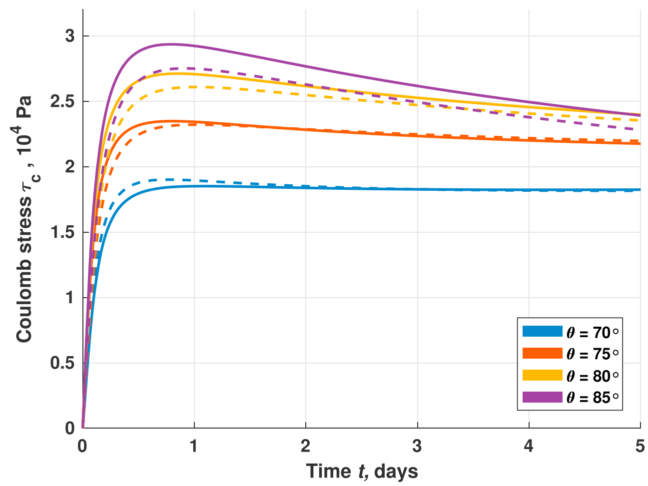

Figure 11. Coulomb stresses for various dip angles. Solid lines dip toward the producer, and dashed lines dip away from the producer.

of compaction and the corresponding straining of faults in the reservoir, as well as by various nonlinear deformation effects not modeled in this study. In terms of the transient effect that is studied here, the variable of interest is the initial reservoir pressure $p_{res,0}$: not only does pressure have a large influence on the hydromechanical properties of the pore fluid, a lower reservoir pressure (i.e., a lower gas density) means that at in situ conditions a larger volume of pore fluid needs to be displaced to achieve a certain production rate in terms of standard cubic meters. Numerical experiments were conducted producing at an equal rate q_{sc} for various reservoir pressures, and Coulomb stress levels were observed to increase substantially; see Figure 16. Decomposition into shear and normal components (Figure 17) reveals that this is caused largely by the increased time lag of the arriving pressure wave, in turn caused by the lower compressibility C_g. This causes the moment at which the minimum normal stress is reached to appear much later, during which time the shear component freely causes Coulomb stress to continue rising steeply.

3.5. Fault Throw

Finally, we investigate the effect of a fault with nonzero fault throw (displacement). Therefore, we include a simulation of a reservoir with a fault dipping toward the producer at $\theta = 85°$, positioned at $r = 100$ m, and with a normal throw of 5% relative to the total height of the reservoir. It should be noted that due to the

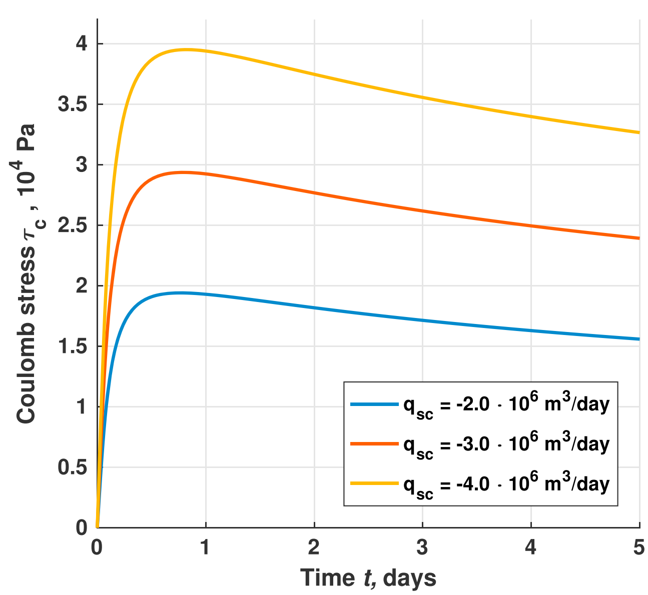

Figure 12. Coulomb stress for an increasing magnitude of the well rate.

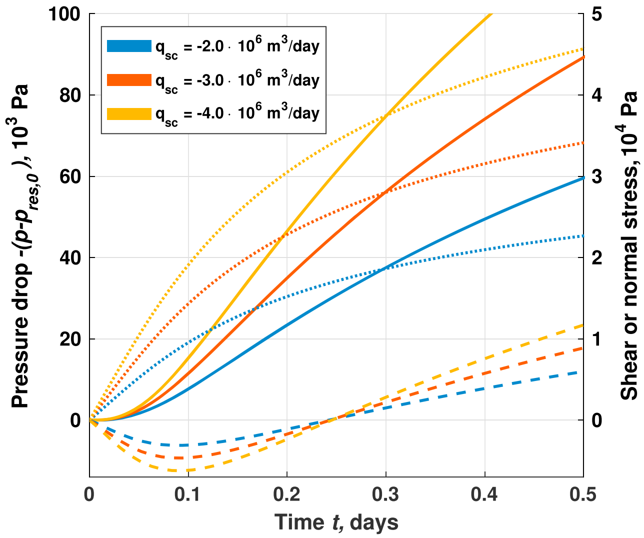

Figure 13. Shear component (dotted) and normal component (dashed) superimposed on pressure drop for the first 0.5 day of production (solid).

radially symmetric description of the problem, this constitutes a fault that forms part of a conical surface wrapped around the producer. Although unphysical geometrically, the behavior of such a system can still provide trends that may apply qualitatively to scenarios of stress concentrations near planar faults as well.

A small throw is chosen so as not to alter the pressure field significantly through the reduction in radial flow area, as that would make comparison to the plane disk scenario more difficult. Moreover, the conical fault would exhibit exceedingly different pressure behavior compared to a geologically realistic scenario. However, we note that, as shown by, for example, Mulders, (2003), Roest and Kuilman (1994), and Wassing et al. (2016), faults most prone to reactivation are those with larger offsets and that, generally, the most critical ones are those with approximately 50% reservoir thickness offset.

Sharp reentrant corners are known to cause singularities in the solution of elliptic partial differential equations (Williams, 1952), leading to unbounded stresses that, in real life, would plastically deform the material. To prevent this effect from dominating the results, reentrant corners were rounded off. Slip-promoting shear

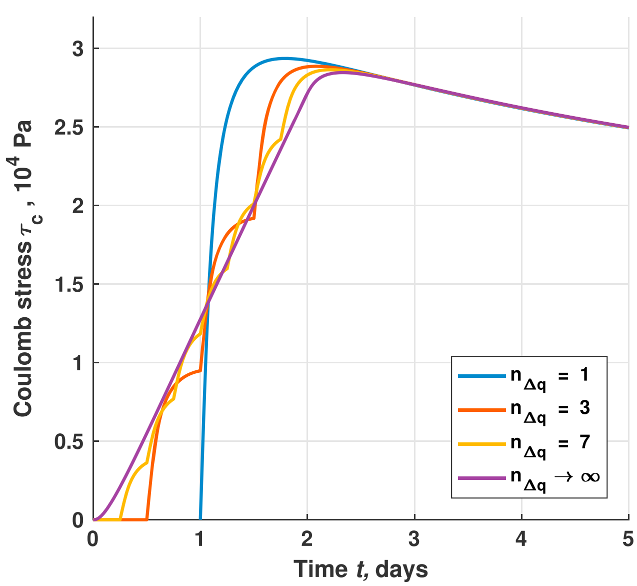

Figure 14. Coulomb stress for an increasing number of well rate increments.

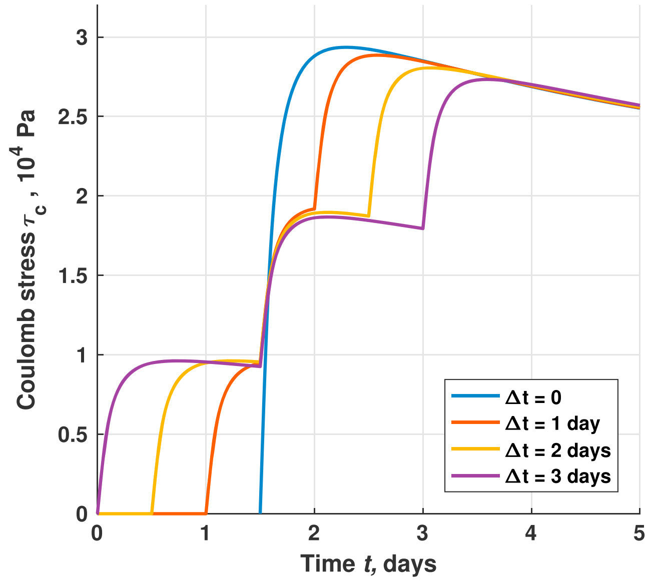

Figure 15. Coulomb stress for an increasing total ramping time.

stresses were observed to concentrate around the geometric irregularities, confirming the observations of Mulders (2003, chapter 4).

After a day of production, it can already be observed that stress concentrations appear around the geometric irregularity (Figure 18), with both a region of elevated and lowered Coulomb stress. Plotting the stress state at the radius of maximum Coulomb stress through time (Figure 19), we find that for the displaced scenario, Coulomb stress at this point is monotonously increasing to levels above the local maximum found in the base case. Examining the shear and normal stresses separately (Figure 20) reveals that both shear and normal stresses grow at a higher rate for the displaced fault, with the former evidently dominating. It is also observed that normal stresses become compressive faster in the displaced case, which is why the base case shows a higher Coulomb stress for the first 30 h of production. Comparison of the local pressure drops for both scenarios shows a near perfect match. Numerical experiments for 20 days of production show a continuation of the trends observed after 5 days, with Coulomb stresses declining for the base case and slowly rising

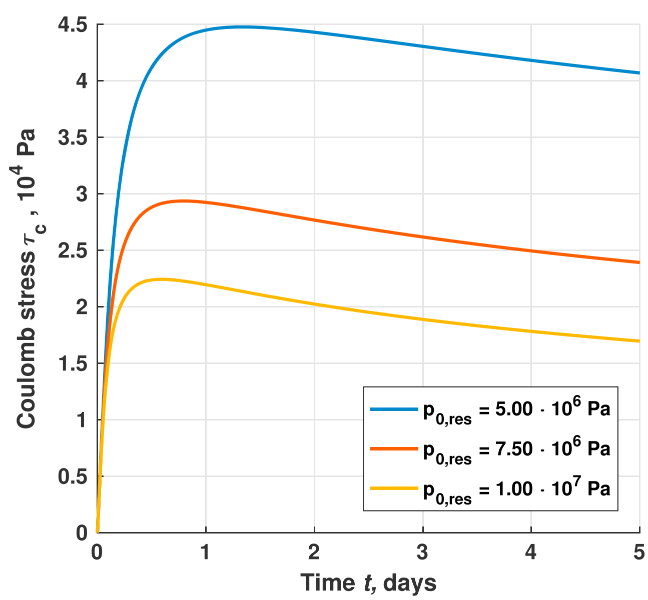

Figure 16. Coulomb stresses in reservoirs of different initial pore pressure.

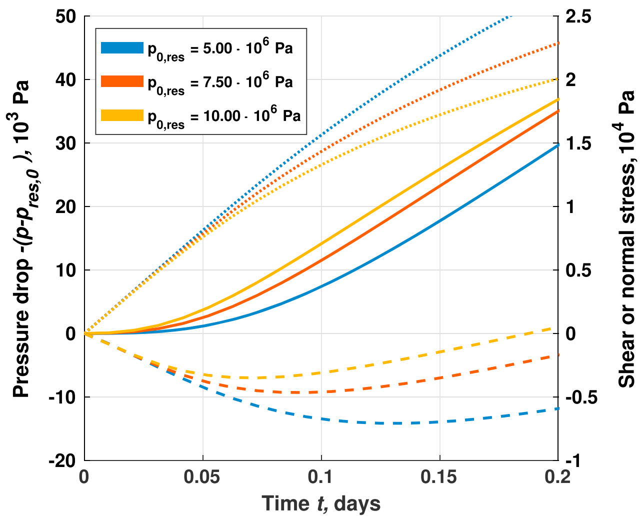

Figure 17. Shear component (dotted) and normal component (dashed) superimposed on pressure drop for the first 0.2 day of production (solid).

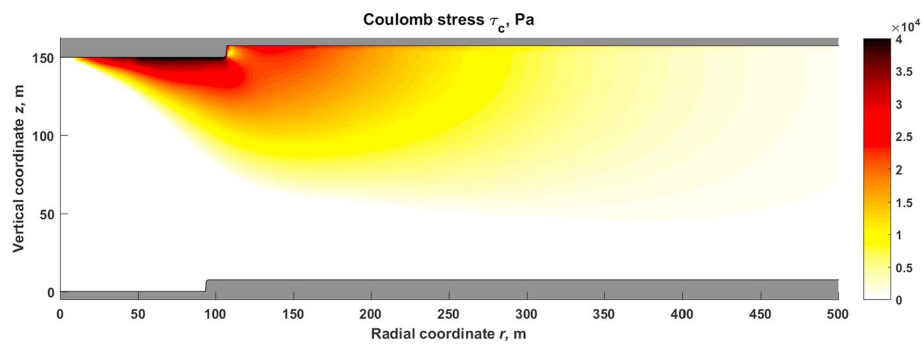

Figure 18. Coulomb stress for a fault with a 5% throw relative to reservoir height, $t = 1$ day.

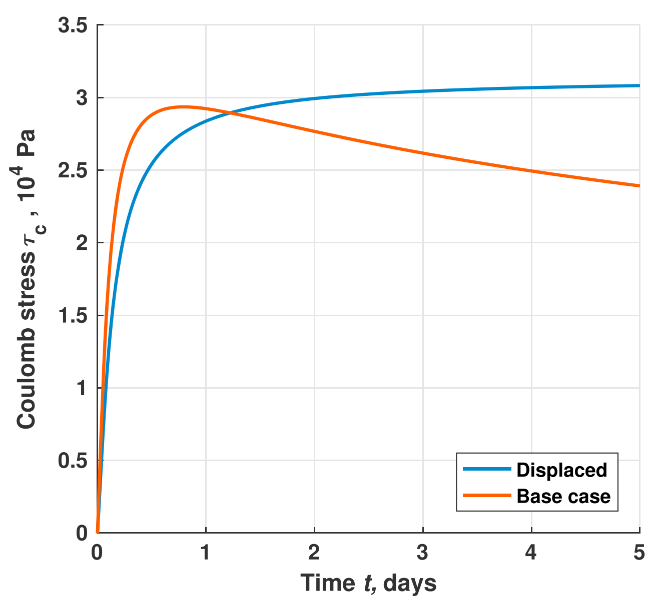

Figure 19. Coulomb stresses found for a fault with a 5% throw compared to the base scenario.

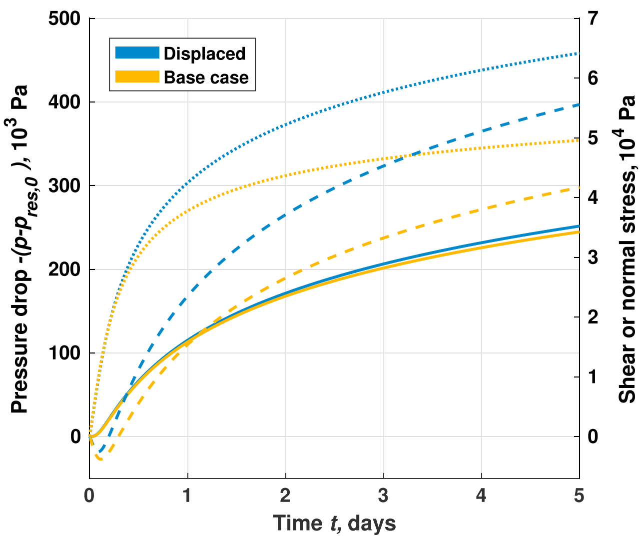

Figure 20. Shear component (dotted) and normal component (dashed) superimposed on pressure drop (solid).

for the displaced fault. It should be noted that this increasing Coulomb stress is observed only locally, with surrounding regions behaving rather more like the base case.

4. Discussion

The reservoir model used in this study is a simplified one, assuming linear elastic behavior, homogeneity in rock properties (within geological strata), and a single pore fluid (gas). While complex real-world subsurface systems will produce at best quantitatively different outcomes, the idealized description used in this study provides insight into the mechanisms behind some of the obtained results. The range of validity is thereby restricted to relatively short time periods (in the order of days) during which the transient slow poroelastic effects of suddenly increasing well rates influence the Coulomb stresses in nearby faults. The recent results of Zbinden et al. (2017) indicate that two-phase (gas-water) flow and, in particular, the slow propagation of fluid pore pressures in response to well shut-in or reinjection may have significant effects at much larger timescales.

4.1. Existence and Mechanisms of Transient Stress Effects

The phenomenon that a sudden change in well rate causes an extra stress effect that may trigger seismicity (Segall & Lu, 2015; Shapiro et al., 2013) was indeed observed: Coulomb stresses showed a local maximum in both time and space. The existence and location of the spatial maximum can be explained in the vertical dimension by the importance of the sign of the shear component and the fact that shear stresses are greatest on the vertical limits of the reservoir. The reason for the maximum in the radial dimension is that the region of highest shear (i.e., close to the wellbore) is also the region of highest normal stress, with normal stresses rising to very high levels as r approaches r_w. This trade-off means that for higher friction coefficients μ_f, the spatial maximum will likely move to a location more distal from the wellbore.

The explanation for the temporal maximum became evident when the shear and normal components of stress were observed separately, as elastic coupling of the rock matrix initially causes a state of relative tension to exist in the region where pore pressure has not yet dropped. This phenomenon can also explain why more steeply dipping faults show the strongest transient effect, both in terms of magnitude and prominence. The asymmetry with respect to dip direction is caused by the asymmetry of the state of shear stress σ_{rz}: the upper half of the reservoir exhibits greater stress magnitudes than the bottom due to the different elastic properties found in the underburden and overburden. As dip angle increases, this asymmetry should become more evident in the Coulomb stress, as is indeed observed.

It should be noted that the effects described seem fundamental and not an artifact of the idealized geometry or discretization of the problem. In terms of unincorporated physics, the simplified linear elastic description of the system is an approach widely used for timescales and deformations exceeding ours by several orders of magnitude. The assumption that $\frac{1}{K} \ll \phi C_g$ was monitored and satisfied for all simulations. Taking all this into account, we have no reason to assume that the effects described will not also occur in a real reservoir setting. A sensitivity study (not reported here), which separately altered the elastic moduli of the reservoir or the surrounding rock, showed that the effect of increased Coulomb stress increased for more elastic reservoir rock and more stiff surroundings.

Although the transient stress effects were indeed observed in our simulations, magnitudes of Coulomb stress, and also of its two components, were only in the order of a few 10^4 Pa. This appears very small, especially when compared to the ambient stress levels, which are 3 orders of magnitude higher. Note that at the time and place where the maximum Coulomb stress occurs (i.e., after approximately 1 day at a radius of around 100 m) the drop in reservoir pressure is also only about 10^5 Pa; see Figure 3.

In the Groningen field, production wells are concentrated in clusters of, typically, 10 to 12 near-vertical wells at mutual distances of approximately 70 m. In theory, the clusters could increase the transient stress effect, because the near-linear poroelastic theory in terms of pseudopressures, which forms the basis for our paper, allows for linear superposition of the observed stresses. The detailed additive effect of interaction between the transients in a cluster would require further study at a level of complexity beyond our model. However, the production rate of $q_{sc} = -3.0 \cdot 10^6$ m^3/d as used in our study could be considered an extremely high rate in a single well or, more realistically, the combined rate in a virtual well representing the wells in a typical cluster. It seems therefore unlikely that the combined effect, in terms of Coulomb stresses in nearby faults, would be much higher than observed in our simulation.

Moreover, a geometric irregularity in the form of a fault with a relatively small displacement caused (Coulomb) stress concentrations of a magnitude that quickly exceeded the local maximum found for the disk-shaped geometry, while still climbing monotonously after 20 days of production. There is a key difference between the triggering effects in the base case and in the case with a displaced fault: the Coulomb stress maximum in the base case is a truly transient effect that results from suddenly increasing the well rate, whereas the growth of the Coulomb stress in the displaced fault will happen anyway with increasing depletion, irrespective of sudden or gradual opening-up of the well.

We can therefore conclude that suddenly opening-up a well (or a cluster of wells) indeed results in a poroelastic transient that can trigger an already (near)critically stressed fault. As discussed in section 1, fault criticality in the Groningen field may result from poroelastic compaction, differential depletion, or, most likely, the stress concentration effect in faults having nonzero offsets. In the latter case the gradual reduction in pressure resulting from production will result in a gradual increase in Coulomb stresses in the displaced faults that will therefore most likely trigger seismicity anyway in those faults that are already near critically stressed. The gradual opening-up of wells in a real faulted reservoir that is being near continuously depleted, as is the case for the Groningen field, will therefore at best delay the triggering of seismic events but will most likely not prevent them from happening.

We note that there may be other operational reasons to justify the gradually opening-up of wells, such as the avoidance of sand production. We also note that the transient effect considered in our study is restricted to timescales in the order of days. The potential beneficial effect of minimizing seasonal fluctuations in gas production is therefore not captured by our analysis and requires further investigation, which should include aspects like two-phase (gas/water) flow and the constitutive relations governing fault friction under stress reversals.

5. Conclusions

1. A hypothesized transient maximum in slip-promoting stresses following a sudden increase in production rate is observed in our simulations.
2. The underlying cause is the time required for the pressure disturbance to reach a certain radius, during which the comparatively instantaneous elastic coupling through the rock matrix induces a state of relative radial tension and growing shear stress. As pore fluid pressure drops, effective normal stresses become compressive and subsequently grow to first increase and then lower the Coulomb stress.
3. The effect is strengthened with increasing dip angle, increasing well rate, and decreasing reservoir pressure. Moreover, in clusters of production wells the arrival of pressure transients of several wells may coincide, thus magnifying the triggering effect. Quantifying the effect of two-phase (gas-water) flow will require further study.
4. A gradual or stepwise buildup to the operating rate was observed to lower the maximum Coulomb stress, with a larger time window being of much greater value than an increased number of rate increments.
5. Although showing the described behavior, both Coulomb stress and its components appear small to the point of insignificance, with ambient stresses exceeding them by 3 orders of magnitude.
6. A small geometric irregularity in the form of a fault with a 5% throw relative to reservoir height caused (Coulomb) stress concentrations to quickly and monotonously build up to levels far exceeding the observed maximum in the disk-shaped reservoir. Larger fault offsets will lead to even larger stress concentrations.
7. The growth of the Coulomb stress in a fault with offset will happen anyway with increasing depletion (irrespective of sudden or gradual opening-up of the well), whereas the Coulomb stress maximum as observed in a reservoir with zero-throw faults is a truly transient effect that results from suddenly increasing the well rate.

8. The gradual opening-up of wells in a real faulted reservoir that is being near continuously depleted, as is the case for the Groningen field, will therefore at best delay the triggering of seismic events but will most likely not prevent them from happening.

Acknowledgments
The second author acknowledges financial support by the Institute for Pure and Applied Mathematics (IPAM) at the University of California Los Angeles (UCLA) for his extended stay at IPAM during the Long Program on Computational Issues in Oil Field Applications (20 March to 9 June 2017) during which part of this work was performed. Data used as model input are referenced within this manuscript. Matlab code used to generate the results is available by contacting the second author at j.d.jansen@tudelft.nl.

References

Al-Hussainy, R., Ramey Jr., H. J., & Crawford, P. B. (1966). The flow of real gases through porous media. *Journal of Petroleum Technology*, *18*(5), 624–636.

Azizi, N., Behbahani, R., & Isazadeh, M. A. (2010). An efficient correlation for calculating compressibility factor of natural gases. *Journal of Natural Gas Chemistry*, *19*, 642–645.

Bear, J., & Corapcioglu, M. Y. (1981). Mathematical model for regional land subsidence due to pumping: 2. Integrated aquifer subsidence equations for vertical and horizontal displacements. *Water Resources Research*, *17*(4), 947–958.

Biot, M. A. (1941). General theory of three-dimensional consolidation. *Journal of Applied Physics*, *12*, 155–164.

Biot, M. A. (1956). Theory of propagation of elastic waves in a fluid-saturated porous solid. *Journal of the Acoustical Society of America*, *28*, 168–191.

Bourne, S. J., Oates, S. J., van Elk, J., & Doornhof, D. (2014). A seismological model for earthquakes induced by fluid extraction from a subsurface reservoir. *Journal of Geophysical Research: Solid Earth*, *119*, 8991–9015. https://doi.org/10.1002/2014JB011663

Carter, J. P., & Booker, J. R. (1982). Elastic consolidation around a deep circular tunnel. *International Journal of Solids and Structures*, *18*(12), 1059–1074.

Carr, N. L., Kobayashi, R., & Burrows, D. B. (1954). Viscosity of hydrocarbon gases under pressure. *Journal of Petroleum Technology*, *6*(10), 47–55.

Cheng, A. H. D. (2016). Theory and applications of transport in porous media, *Poroelasticity* (Vol. 27). Switzerland: Springer.

Chessa, J. (2002). *Programming the finite element method with Matlab*. Evanston, IL: Northwestern University.

Cleary, M. P. (1977). Fundamental solutions for a fluid-saturated porous solid. *International Journal of Solids and Structures*, *13*(9), 785–806.

Clegg, M. W. (1967). Some approximate solutions of radial flow problems associated with production at constant well pressure. *Society of Petroleum Engineers Journal*, *7*(1), 32–41.

Dahm, T., Cesca, S., Hainzl, S., Braun, T., & Krüger, F. (2015). Discrimination between induced, triggered, and natural earthquakes close to hydrocarbon reservoirs: A probabilistic approach based on the modeling of depletion-induced stress changes and seismological source parameters. *Journal of Geophysical Research: Solid Earth*, *120*, 2491–2509. https://doi.org/10.1002/2014JB011778

Dempsey, D., & Suckale, J. (2017). Physics-based forecasting of induced seismicity at Groningen gas field, the Netherlands. *Geophysical Research Letters*, *44*, 7773–7782. https://doi.org/10.1002/2017GL073878

De Waal, J. A., Muntendam-Bos, A. G., & Roest, J. P. A. (2015). Production induced subsidence and seismicity in the Groningen gas field—Can it be managed?. In K. Daito & D. Galloway (Eds.), *Prevention and mitigation of natural and anthropogenic hazards due to land subsidence* (Vol. 372, pp. 129–139): Proceedings International Association of Hydrological Sciences, Göttingen, Germany: Copernicus Publications.

Ellsworth, W. L. (2013). Injection-induced earthquakes. *Science*, *341*(6142), 1225942.

Grasso, J. R. (1992). Mechanics of seismic instabilities induced by the recovery of hydrocarbons. *Pure and Applied Geophysics*, *139*, 507–534.

Grigoli, F., Cesca, S., Priolo, E., Rinaldi, A. P., Clinton, J. F., Stabile, T. A., … Dahm, T. (2017). Current challenges in monitoring, discrimination, and management of induced seismicity related to underground industrial activities: A European perspective. *Reviews of Geophysics*, *55*, 310–340. https://doi.org/10.1002/2016RG000542

Helm, D. C. (1994). Horizontal aquifer movement in a Theis-Thiem confined system. *Water Resources Research*, *30*(4), 953–964.

Hsieh, P. A., & Cooley, R. L. (1995). Comment on 'Horizontal aquifer movement in a Theis-Thiem confined system' by Donald C. Helm. *Water Resources Research*, *31*(12), 3107–3111.

Jacob, C. E. (1940). On the flow of water in an elastic artesian aquifer. *Eos, Transactions of the American Geophysical Union*, *21*(2), 574–586.

Karimi-Fard, M., Durlofsky, L. J., & Aziz, K. (2003). An efficient discrete fracture model applicable for general purpose reservoir simulators, *Proceedings of the SPE reservoir simulation symposium* pp. 3–5). Houston, TX: Society of Petroleum Engineers.

Kirchhof, G. (1894). *Vorlesungen über mathematische Physik: Band IV - Theorie der Wärme*. Leipzig: Teubner.

Lele, S. P., Hsu, S.-Y., Garzon, J. L., DeDontney, N., Searles, K. H., Gist, G. A., … Dale, B. A. (2016). Geomechanical modeling to evaluate production-induced seismicity at Groningen field, *Proceedings of the Abu Dhabi International Petroleum Exhibition and Conference* (Paper SPE-183554-MS, pp. 1–18). Abu Dhabi, UAE: Society of Petroleum Engineers.

Lucas, K. (1981). Die Druckabhängigkeit der Viskosität von Flüssigkeiten - ene einfache Abschätzung. *Chemie Ingenieur Technik*, *53*(12), 959–960.

McGarr, A., Simpson, D., & Seeber, L. (2002). Case histories of induced and triggered seismicity. In W. K. H. Lee et al. (Eds.), *International handbook of earthquake and engineering seismology, Part A* (Vol. 81A, pp. 647–661). London: Academic Press.

Monfared, K. A., & Rothenburg, L. (2015a). A numerical study of poroelastic geomechanical processes during fluid injection in confined geological reservoirs, *Proceedings of the 15th Pan-American Conference on Soil Mechanics and Geotechnical Engineering (PCSMGE)/8th South American Congress on Rock Mechanics (SCRM), 'from fundamentals to applications in geotechnics', Buenos Aires* (pp. 1207–1214). Amsterdam: IOP Press.

Monfared, A. K., & Rothenburg, L. (2015b). Poroelastic stress modifications surrounding a fully-penetrating injection well. *Journal of Petroleum Science and Engineering*, *135*, 660–670.

Mulders, F. M. M. (2003). Modelling of stress development and fault slip in and around a producing gas reservoir (PhD Thesis). Delft, The Netherlands: Delft University of Technology.

Nederlandse Aardolie Maatschappij (2016). Winningsplan Groningen Gasveld. Retrieved from http://www.nam.nl/gas-en-oliewinning/groningen-gasveld/winningsplan-groningen-gasveld.html

Nepveu, M., Van Thienen-Visser, K., & Sijacic, D. (2016). Statistics of seismic events at the Groningen field. *Bulletin of Earthquake Engineering*, *14*, 3343–3362.

Orlic, B., & Wassing, B. B. T. (2013). A study of stress change and fault slip in producing gas reservoirs overlain by elastic and viscoelastic caprocks. *Rock Mechanics and Rock Engineering*, *46*, 421–435.

Pijpers, F. P. (2017). Interim report: Correlations between reservoir pressure and earthquake rate (*Statistics Netherlands*). Scientific paper 2017|04, The Hague, The Netherlands.

Roest, J. P. A., & Kuilman, W. (1994). Geomechanical analysis of small earthquakes at the Eleveld gas reservoir, *Proceedings of the SPE-IISRM rock mechanics in petroleum engineering conference* (Paper SPE 28097, pp. 573–580). Delft, Netherlands.

Rudnicki, J. W. (1986). Fluid mass sources and point forces in linear elastic diffusive solids. *Mechanics of Materials*, *5*(4), 383–393.

Sanz, P. F., Lele, S. P., Searles, K. H., Hsu, S.-Y., Garzon, J. L., Burdette, J. A., … Hector, P. D. (2015). Geomechanical analysis to evaluate production-induced fault re-activation at Groningen field, *Proceedings of the SPE Annual Technical Conference Exhibition* (Paper SPE 174942-MS, pp. 1–19). Houston, TX.

Segall, P. (1989). Earthquakes triggered by fluid extraction. *Geology*, *17*(10), 942–946.

Segall, P., & Fitzgerald, S. (1998). A note on induced stress changes in hydrocarbon and geothermal reservoirs. *Tectonophysics*, *289*(1–3), 117–128.

Segall, P., & Lu, S. (2015). Injection-induced seismicity: Poroelastic and earthquake nucleation effects. *Journal of Geophysical Research: Solid Earth*, *120*, 5082–5103. https://doi.org/10.1002/2015JB012060

Shapiro, S. A., Krüger, O. S., & Dinske, C. (2013). Probability of inducing given-magnitude earthquakes by perturbing finite volumes of rocks. *Journal of Geophysical Research: Solid Earth*, *118*, 3557–3575. https://doi.org/10.1002/jgrb.50264

Shapiro, S. A. (2015). *Fluid-induced seismicity*. Cambridge: Cambridge University Press.

Sternberg, Y. M. (1969). Some approximate solutions of radial flow problems. *Journal of Hydrology*, *7*(2), 158–166.

Theis, C. V. (1935). The relation between the lowering of the piezometric surface and rate and duration of a well using groundwater storage. *Eos, Transactions of the American Geophysical Union*, *16*(2), 519–524.

Van Everdingen, A. F., & Hurst, W. (1949). The application of the Laplace transformation to flow problems in reservoirs. *Journal of Petroleum Technology*, *12*(1), 305–324.

Van Thienen-Visser, K., & Breunese, J. N. (2015). Induced seismicity of the Groningen gas field: History and recent developments. *The Leading Edge*, *34*(6), 664–666.

Van Wees, J. D., Buijze, L., Van Thienen-Visser, K., Nepveu, M., Wassing, B. B. T., Orlic, B., & Fokker, P. A. (2014). Geomechanics response and induced seismicity during gas field depletion in the Netherlands. *Geothermics*, *52*, 206–219.

Verruijt, A. (2016). Theory and problems of poroelasticity, Delft University of Technology. Retrieved from http://www.geo.verruijt.net

Wang, H. (2000). *Theory of linear poroelasticity with applications to geomechanics and hydrogeology*. Princeton, NJ: Princeton University Press.

Wassing, B. B. T., Buijze, L., & Orlic, B. (2016). Modelling of fault reactivation and fault slip in producing gas fields using a slip-weakening friction law, *Proceedings of the 50th US Rock Mechanics/Geomechanics Symposium* (Paper ARMA 16-658, pp. 1–11). Houston, TX.

Williams, M. L. (1952). Stress singularities resulting from various boundary conditions in angular corners of plates in extension. *International Journal of Solids and Structures*, *43*(17), 5100–5109.

Zbinden, D., Pio Renaldi, A., Urpi, L., & Wiemer, S. (2017). On the physics-based processes behind production-induced seismicity in natural gas fields. *Journal of Geophysical Research: Solid Earth*, *122*, 3792–3812. https://doi.org/10.1002/2017JB014003

Zoback, M. D. (2007). *Reservoir geomechanics*. Cambridge: Cambridge University Press.